Linking elastic and electrical properties of rocks using cross-property DEM

P. A. Cilli[1,2,3*] and M. Chapman[1,2]

[1]*Grant Institute, School of GeoSciences, The University of Edinburgh, James Hutton Rd, King's Buildings, Edinburgh, EH9 3FE, UK*
[2]*International Centre for Carbonate Reservoirs, Edinburgh, UK*
[3]*Current address: Department of Earth Sciences, University of Oxford, South Parks Road, Oxford, OX1 3AN, UK*
[*]*Corresponding author: Phillip.Cilli@earth.ox.ac.uk*

This manuscript is a non-peer reviewed preprint submitted to EarthArXiv. The content of subsequent versions may differ slightly. Date submitted: 19/10/2020.

Abstract

Joint electrical-elastic rock physics modelling can be instrumental in lowering uncertainty in subsurface reservoir characterisation. Typical electrical-elastic cross-property models, however, are empirical or require an intermediate step of porosity estimation to link a rock's electrical and elastic moduli, which can be error-prone away from well controls. Another outstanding issue in electrical-elastic modelling is the challenge of predicting a rock's shear modulus and ultimately V_p/V_s ratio from electrical measurements. By reformulating an existing electrical differential effective medium (DEM) theory to embed ellipsoidal pores into a background of matrix material, rather than the typical method of embedding ellipsoidal grains into a background of fluid, we express the model in terms of the geometrical function R, which is present in other electrical ellipsoidal inclusion models. This reformulation is consistent with two other effective conductivity models and shares its geometrical function R with the electrical self-consistent approximation (SCA) model, providing a new mathematical link between electrical DEM and SCA models. Combining this reformulated electrical DEM model and a pre-existing elastic DEM model, we obtain expressions for a rock's effective elastic moduli with respect to effective conductivity. This method is analogous to the more common electrical-elastic modelling stratagem where an electrical model is substituted into an elastic model or vice versa through their shared independent variable, porosity, which is rendered a dummy variable in the process. Modelling the elastic moduli of clay-bearing sandstones using public domain laboratory measurements, there seems to be a weak sensitivity of the model's single parameter, equivalent pore aspect ratio, to clay volume fraction. Furthermore, the uncertainty in shear modulus modelling from conductivity measurements seems weakly sensitive to clay content. By employing the Gardner empirical velocity-density relation for sandstones, we forward model V_p and V_s from electrical measurements in the absence of porosity and density measurements, with accuracy comparable to the Han (1986) empirical V_p/V_s model for mixed sandstones. Our proposed cross-property DEM method generalises mathematically to relate any two of a composite's elastic moduli, electrical conductivity, electrical permittivity, thermal conductivity, magnetic permeability, and diffusion constant due to the equivalence of these properties in inclusion modelling by the universality of the Laplace equation, which underpins the models' constructions. This generalisation of the cross-property DEM model to numerous physical properties leads to a testable hypothesis: the cross-property DEM parameter, aspect ratio, is (or is not) universal when linking a given rock's various physical properties.

1 Introduction

Electrical-elastic multiphysics modelling, for example through the integration of controlled-source electromagnetic (CSEM) data into marine seismic reservoir characterisation workflows, can lead to reduced uncertainty in reservoir characterisation (Alcocer et al., 2013). However, a simple, physics-based, and accurate multiphysics model which links a porous rock's electrical and elastic properties remains elusive. Many existing electrical-elastic relationships are at least partly empirical (Carcione et al., 2007). In addition to this, the majority of workflows which relate a rock's elastic and electrical properties require the estimation of porosity as an intermediate step (e.g., Carcione et al. (2007); Engelmark (2010); Werthmüller et al. (2013)), which can be uncertain away from well control.

Carcione et al. (2007) presented a set of electrical-elastic cross-property models with no explicit porosity terms by substituting pre-existing resistivity-porosity models into pre-existing velocity-porosity models. Chen & Dickens (2009) and Werthmüller et al. (2013) assessed the intrinsic (theoretical) and extrinsic (parametrisation) uncertainties involved in these models, which were generally found to be significant. In fact, Kwon & Snieder (2011) showed the uncertainty in these multiphysics models had a larger contribution to overall uncertainty than that associated with the data. The electrical-elastic Hashin-Shtrikman bounds (Carcione et al., 2007), on the other hand, have no explicit porosity terms and are physically meaningful, but can be too widely spaced to predict the physical properties of any rock in particular.

Estimating the Earth's shear modulus is an important aspect of geophysics at many scales, from understanding the composition of the Earth's mantle (Kennett et al., 1998), to estimating reservoir fluids using V_p/V_s ratios (Hamada, 2004), to geotechnical soil studies (Hussien & Karray, 2015). Estimating a rock's shear modulus from its electrical resistivity, however, is scarcely addressed in the geophysical literature. On the cratonic scale, Jones et al. (2013) proposed a best-fitting linear trend between shear velocity and the reciprocal of the logarithm of resistivity before using this trend to predict V_s from electrical measurements. In the soil sciences, Yasir et al. (2018) estimated the shear modulus of soil in place by first calculating Young's modulus from electrical tomography results using an empirical model, before employing tabulated Poisson's ratios and the equations of linear elasticity to obtain the result. Although some other works do exist which predict V_s from resistivity, their methods are generally not based on first principles physics, require more measurements than resistivity alone, or both. It seems that the problem of modelling a rock's shear modulus from electrical resistivity mea-

surements alone using a simple model based on first principles physics remains unsolved.

Joint electrical-elastic modelling with a single model parameter has been attempted with mixed success (Han et al., 2011a; Wang & Gelius, 2010; Jensen et al., 2013). Notwithstanding, a scrutiny by Han et al. (2016) concluded a new multiphysics model was required to accurately relate the electrical and elastic properties of a porous rock using a single set of model parameters. Werthmüller et al. (2013) note that there is no known direct link between a rock's velocity and resistivity.

In this paper, we present a new form of differential effective medium (DEM) model which relates the electrical and elastic properties of an isotropic, porous rock. The model uses the stratagem of Carcione et al. (2007), where an electrical model is substituted into an elastic model through the common independent variable, porosity, which is rendered a dummy variable in the process. Employing this stratagem in the context of a DEM scheme gives a predictive trend with only one model parameter, inclusion aspect ratio.

The presented electrical-elastic model can be expressed in terms of the geometrical functions $Q^{(*2)}$, $P^{(*2)}$, and $R^{(*2)}$, proposed by Berryman (1980, 1995). We demonstrate that the model is useful in practice by data example, where we accurately model the wet, mixed sandstone core measurements of Han et al. (2011b). We show the single model parameter, effective pore aspect ratio, is weakly sensitive to clay volume fraction when modelling this data set. Likewise, the uncertainty in shear modulus modelling also seems weakly sensitive to clay volume fraction when modelling this data. In addition to this, we demonstrate that one can model a V_p/V_s trend for a collection of mixed, wet sandstones using only electrical conductivity measurements and an empirical velocity-density relation once the model is parameterised, with accuracy comparable to the V_p/V_s model of Han et al. (1986).

To begin, we reformulate the electrical differential effective medium (DEM) model of Mendelson & Cohen (1982) for the case when ellipsoidal fluid-filled pores are embedded in a background of mineral matrix, contrasting with the typical expression which embeds grains into a background of water. Following this, we combine this reformulated electrical DEM expression with the analogous elastic DEM expressions of Berryman (1992) using Carcione's stratagem for cross-property modelling - which in the case of DEM equates to applying the chain rule - to obtain new electrical-elastic DEM expressions. We then test this cross-property DEM model's performance on the laboratory electrical-elastic measurements of Han et al. (2011b), which are made on brine-flooded sandstone cores

from multiple localities, having a range of clay and pore volume fractions. We estimate the optimal parameters which model the rock's bulk and shear modulus from resistivity measurements, and investigate the effect of clay content on the model's parametrisation and uncertainty. Finally, we predict a V_p/V_s trend for mixed, wet sandstones in the absence of porosity and density measurements using the modelled elastic moduli and the Gardner et al. (1974) velocity-density relation for sandstones.

2 Model Derivation

2.1 Electrical modelling

Electrical inclusion modelling was first popularised by Maxwell Garnett (1904), who proposed an effective medium approximation to calculate the electrical properties of a material containing spherical inclusions. This was followed by Bruggeman (1935), who proposed an electrical DEM model for the same material. By devising a DEM model which embedded fractal-layered insulating spherical grains into a background initially made of water, Sen et al. (1981) derived Archie's (Archie, 1942) first law with cementation exponent $m = 1.5$ and tortuosity $a = 1$.

Recognising it is unrealistic to approximate pores, grains, and inclusions in general with spheres, ellipsoidal inclusions became favoured when analytically modelling the electrical properties of composite materials due to their ability to approximate reality more accurately while still producing analytically tractable models. Polder & Van Santeen (1946) estimated the average electrical properties of an isotropic medium containing randomly oriented ellipsoidal inclusions which are assumed to be non-interacting, before Frank (1963) calculated the effective electric field in a medium containing a single homogeneous ellipsoid with principal axes arbitrarily aligned with respect to the incident electric field. Extending the work of Sen et al. (1981), Mendelson & Cohen (1982) developed a DEM model to calculate the effective electrical properties of a medium containing many arbitrarily oriented ellipsoidal inclusions in a uniform, static electric field.

Arguably the most renowned aspect of the DEM model of Mendelson & Cohen (1982), abbreviated to "M&C" henceforth, is a subsidiary result: by setting the grain conductivity to zero, fluid conductivity to that of water, and letting ellipsoidal grains be randomly oriented, M&C's electrical DEM model takes the form of Archie's (Archie, 1942) first law:

$$\sigma^* = \sigma_w \phi^m \,. \tag{1}$$

Parameter σ^* is the rock's overall conductivity, σ_w is the saturating water's conductivity, and m is the cementation factor. We note tortuosity factor a, a common coefficient of Archie's first law (Glover, 2016), can be said to be unity in equation 1, as is also derived in the electrical DEM model of Sen et al. (1981) for spherical grains. Importantly, M&C showed m is a function of grain aspect ratio α, agreeing with observations that m depends on grain shape (e.g., Salem & Chilingarian (1999)).

M&C consider a rock with background material volume fraction (porosity) ϕ, background material conductivity σ_2, and inclusion (i.e., grain) conductivity σ_1. M&C's DEM model in its most general form for inclusions of a single aspect ratio is then:

$$d\sigma^* = -\frac{d\phi}{\phi} \left\langle (\sigma_1 - \sigma^*) \left[1 + (\sigma^*)^{-\frac{1}{2}} \boldsymbol{\Theta}_1 (\sigma^*)^{-\frac{1}{2}} (\sigma_1 - \sigma^*) \right]^{-1} \right\rangle ; \tag{2}$$

where angled brackets denote an average over all inclusion orientations and $\boldsymbol{\Theta}_1$ is a 3×3 matrix, such that:

$$\boldsymbol{\Theta}_1 = \mathbf{R}\mathbf{L}\mathbf{R}^{-1} \,. \tag{3}$$

Matrix $\boldsymbol{\Theta}_1$ (Frank, 1963) contains the effective depolarisation factors of an ellipsoidal inclusion of phase 1 which is arbitrarily rotated with respect to an incident electric field. Matrix $\mathbf{L}$ is the diagonal matrix with the ellipsoid's three depolarisation factors L_p, $p \in \{1, 2, 3\}$, along its diagonal. Depolarisation factors L_p (e.g., Osborn (1945)) are the shape-dependent scalars which map from the scalar component of an external electric field applied along the ellipsoid's p^{th} axis, $\mathscr{E}_p$, to the ellipsoid's dipole moment along its p^{th} axis, $\mathscr{P}_p$, through the relation:

$$\mathscr{P}_p = \frac{\mathscr{E}_p V}{4\pi L_p} \,, \tag{4}$$

where V is the ellipsoid's volume. Matrix $\mathbf{L}$ is has trace unity, and $\mathbf{R}$ is an orthogonal matrix. In the case of randomly oriented ellipsoidal grains, $\mathbf{R} = \mathbf{I}$ and the rock's effective conductivity is isotropic, presuming an isotropic background conductivity. In this paper, we only consider the isotropic case and so set $\boldsymbol{\Theta}_1 = \mathbf{L}$ henceforth.

To derive equation 1, M&C make the approximation that grains are perfect resistors by setting $\sigma_1 = 0$ in equation 2 and obtain the differential equation:

$$\frac{d\sigma^*}{\sigma^*} = m\frac{d\phi}{\phi}\,; \tag{5}$$

with cementation factor m:

$$m = \frac{1}{3}\sum_{p=1}^{3}\left\langle [1 - L_p]^{-1}\right\rangle\,. \tag{6}$$

Taking the average of equation 6 over all grain orientations and integrating with the boundary condition $\sigma^*\left(\phi = 1\right) = \sigma_2$ yields equation 1 with $\sigma_2 = \sigma_w$.

Our current aim is to reformulate the DEM model of equations 5 and 6 with reversed phases, embedding fluid-filled pores into a background of matrix material. To do this, we change the variable ϕ to $(1 - \phi)$ and interchange subscripts 1 and 2 in equation 2 to obtain:

$$\frac{d\sigma^*}{\sigma^* - \sigma_2} = \bar{m}\frac{d\left(1-\phi\right)}{\left(1-\phi\right)}\,; \tag{7}$$

where we define $\bar{m}$ as:

$$\bar{m} = \frac{1}{3}\sum_{p=1}^{3}\left\langle \left[1 + \left(\frac{\sigma_2}{\sigma^*} - 1\right)L_p\right]^{-1}\right\rangle\,. \tag{8}$$

Equations 7 and 8 are a reformulation of equations 5 and 6 respectively, here with pores embedded into a background of matrix material.

Changing the independent variable in equation 7, we obtain the reformulation of M&C's electrical DEM model with ellipsoidal pores embedded into a background of matrix material:

$$\frac{d\sigma^*}{d\phi} = \frac{\left(\sigma_2 - \sigma^*\right)\bar{m}}{\left(1-\phi\right)}\,. \tag{9}$$

By considering spheroidal inclusions, we drop the subscript p in depolarisation factors L_p, calling the principal depolarisation factor L, and the two degenerate factors $(1 - L)/2$, as the trace of $\mathbf{L}$ is unity.

Parameter $\bar{m}$ from equation 8 for randomly oriented spheroidal inclusions is thus:

$$\bar{m} = \frac{1}{3}\sigma^* \left[\frac{4}{\sigma^* + \sigma_2 + L\left(\sigma^* - \sigma_2\right)} + \frac{1}{\sigma^* - L\left(\sigma^* - \sigma_2\right)} \right] ; \tag{10}$$

The function $R^{(*2)}$ proposed by Berryman (1995) for the electrical Clausius-Mossotti and self-consistent approximation models with a single phase of randomly oriented spheroidal inclusions is defined as:

$$\begin{aligned} R^{(*2)} &= \frac{1}{9} \left[\frac{4}{\sigma^* + \sigma_2 + L\left(\sigma^* - \sigma_2\right)} + \frac{1}{\sigma^* - L\left(\sigma^* - \sigma_2\right)} \right] ; & (11) \\ &= \frac{\bar{m}}{3\sigma^*} . & (12) \end{aligned}$$

Thus, by equations 9 and 12, the DEM model of M&C can now be expressed in terms of the geometric function $R^{(*2)}$:

$$\frac{d\sigma^*}{d\phi} = 3\sigma^* \frac{\left(\sigma_2 - \sigma^*\right) R^{(*2)}}{\left(1 - \phi\right)} . \tag{13}$$

As an aside, we note the two-phase self-consistent electrical model for spheroidal pores of Berryman (1995) can be formulated in terms of $\bar{m}$:

$$\frac{\phi\left(\sigma_2 - \sigma^*\right)\bar{m}}{3\sigma^*} = 0 . \tag{14}$$

This may be of interest if a physically meaningful link between $\bar{m}$ and a rock's petrophysical properties is found, as exists with the analogous m (e.g., Salem & Chilingarian (1999)) but is not so obvious with the SCA model's typical geometrical function $R^{(*2)}$.

We also see equation 9 reduces to the electrical DEM model of Bruggeman (1935) in the special case when $L = 1/3$. This result is expected as the model of Mendelson & Cohen (1982) is consistent with that of Sen et al. (1981) in the case of spherical inclusions, which in turn is consistent with that of Bruggeman (1935).

We only require equation 9 to obtain our proposed, joint electrical-elastic DEM expressions. For completeness, however, we integrate equation 9 here to obtain an expression analogous to Archie's first law as derived by M&C. For simplicity, we make the approximation that $\bar{m}$ in equation 10 is constant in σ^* by assuming $\sigma^* \ll \sigma_2$, as is often the case in rocks with fluid-filled pores. However, equation 9 can be integrated analytically with σ^*-dependent $\bar{m}$ as defined in equation

10 if desired. Integrating equation 9 with boundary condition $\sigma^*(\phi = 0) = \sigma_1$, we find the analogous equation to M&C's expression of Archie's first law:

$$\frac{\sigma_2 - \sigma^*}{\sigma_2 - \sigma_1} = (1 - \phi)^{\bar{m}} \ . \tag{15}$$

2.2 Elastic modelling

Berryman (1992) presented a DEM model which estimates the effective elastic moduli of a dilute dispersion of randomly oriented ellipsoidal inclusions in an isotropic background material by the coupled equations:

$$\frac{dK^*}{d\phi} = \frac{(K_2 - K^*)\, P^{(*2)}}{(1 - \phi)} \, ; \tag{16}$$

$$\frac{d\mu^*}{d\phi} = \frac{(\mu_2 - \mu^*)\, Q^{(*2)}}{(1 - \phi)} \, ; \tag{17}$$

where K and μ denote bulk and shear moduli respectively and ϕ represents inclusion volume fraction. Sub- and superscripts 1 and 2 represent background and inclusion phases respectively, while $*$ denotes the effective properties of the composite. Functions $P^{(*2)}$ and $Q^{(*2)}$ are defined explicitly by Berryman (1980) for the arbitrary spheroidal inclusion. Functions $P^{(*2)}$ and $Q^{(*2)}$ are similar to functions $\bar{m}$ and $R^{(*2)}$ in that they depend on the inclusion aspect ratio α, and the inclusions', as well as the material's effective physical properties. Analogous to the boundary condition of equation 7, equations 16 and 17 are solved with boundary conditions $K^*(\phi = 0) = K_1$ and $\mu^*(\phi = 0) = \mu_1$.

2.3 Electrical-elastic modelling using cross-property DEM

Dividing equations 16 and 17 by equation 9 - that is, employing the chain rule - we obtain a set of coupled differential equations which relate the electrical and elastic properties of a two-phase, isotropic, linearly elastic, electrically conductive composite:

$$\frac{dK^*}{d\sigma^*} = \left(\frac{K_2 - K^*}{\sigma_2 - \sigma^*}\right) \frac{P^{(*2)}}{\bar{m}} \, ; \tag{18}$$

$$\frac{d\mu^*}{d\sigma^*} = \left(\frac{\mu_2 - \mu^*}{\sigma_2 - \sigma^*}\right) \frac{Q^{(*2)}}{\bar{m}} \, . \tag{19}$$

Porosity is rendered a dummy variable when the chain rule is applied, meaning equations 18 and 19 contain no porosity terms.

By equation 12, equations 18 and 19 can be expressed in terms of $P^{(*2)}$, $Q^{(*2)}$, and $R^{(*2)}$:

$$\frac{dK^*}{d\sigma^*} = \frac{1}{3\sigma^*}\left(\frac{K_2 - K^*}{\sigma_2 - \sigma^*}\right)\frac{P^{(*2)}}{R^{(*2)}}\,; \tag{20}$$

$$\frac{d\mu^*}{d\sigma^*} = \frac{1}{3\sigma^*}\left(\frac{\mu_2 - \mu^*}{\sigma_2 - \sigma^*}\right)\frac{Q^{(*2)}}{R^{(*2)}}\,. \tag{21}$$

The boundary conditions of equations 18 and 19, or 20 and 21, are:

$$K^*\left(\sigma^* = \sigma_1\right) = K_1\,; \tag{22}$$

$$\mu^*\left(\sigma^* = \sigma_1\right) = \mu_1\,. \tag{23}$$

The key conceptual difference between these cross-property DEM expressions and a typical electrical or elastic DEM model is that in the cross-property method, the porosity added in each rock-building iteration is not $d\phi$, but the unknown pore volume fraction which increments the rock's effective conductivity by $d\sigma^*$. These cross-property DEM expressions are correct in both the high and low porosity limit even though porosity is rendered a dummy variable.

2.4 Generalised cross-property DEM

The Laplace equation governs the elastic and electric fields with a low frequency source located at infinity, as is the assumption of typical DEM models (Choy, 2016). The universality of the Laplace equation suggests other physical properties can be modelled by DEM with mathematical equivalence; namely, thermal conductivity, electrical permittivity, magnetic permeability, and diffusion constant. Table 1, adapted from Choy (2016), presents the additional physical properties which can be modelled with mathematical equivalence to the electrical resistivity inclusion problem. It follows from this equivalence that modelling using cross-property DEM also extends to any combination of two properties from Table 1, as well as a rock's elastic moduli and electrical resistivity.

As an example of the extension of cross-property DEM beyond electrical-elastic modelling, we derive and present the cross-property DEM equations for

thermal-electrical and thermal-elastic modelling in Appendix A (equations 27 to 29). An interesting feature of this generalised cross-property modelling by cross-property DEM is that all models which do not include elastic properties are governed by a single differential equation (e.g., equation 27), meaning mapping both ways between any two non-elastic properties requires only a single differential equation (and its reciprocal).

3 Laboratory Data Modelling

3.1 Elastic Moduli Modelling

To test the proposed electrical-elastic DEM model, we use the laboratory data set of Han et al. (2011b). This data set is comprised of simultaneous electrical and elastic laboratory measurements made on 63 sandstone cores collected from the UK and China. At least eight minerals are present in the cores, including quartz, four clay minerals, two feldspar minerals, and carbonates. The experiments were conducted by Han et al. (2011b) with a saturating brine concentration of 35 g/L and a pore fluid pressure of 5 MPa. The electrical resistivity measurements had a low-frequency (2 Hz) source, as is of interest in Controlled Source Electromagnetism (CSEM) studies. Core porosity was measured by helium porosimetry, and mineralogy was determined by whole rock X-ray diffraction. The samples were maintained at 19 ± 1 degrees Celsius throughout experiments. Brine-saturated compressional and shear wave velocities were measured at 1.0 MHz and 0.7 MHz respectively.

Velocities were measured at various effective pressures, ranging from 8-60 MPa (Han et al., 2011b). We study the measurements made at 20 MPa in this paper. This is a relatively low pressure, and microcracks are more likely to be present in these samples when compared to higher pressures. The presence of these microcracks would increase the rock's equivalent inclusion eccentricity when compared to a rock at higher pressure. Open microcracks may also allow for squirt flow over a certain frequency band (Mavko & Jizba, 1991; Dvorkin & Nur, 1993; Chapman et al., 2002). However, these factors are not of concern in this study as all measurements analysed are made at constant pressure and frequency.

We study only measurements from the subset of 30 cores which have quartz content greater than 60% volume fraction. We refer to this subset of measurements as the "Han" data henceforth. By considering only these measurements, we ensure mineralogy is quartz-dominated. Accordingly, we model all data assuming

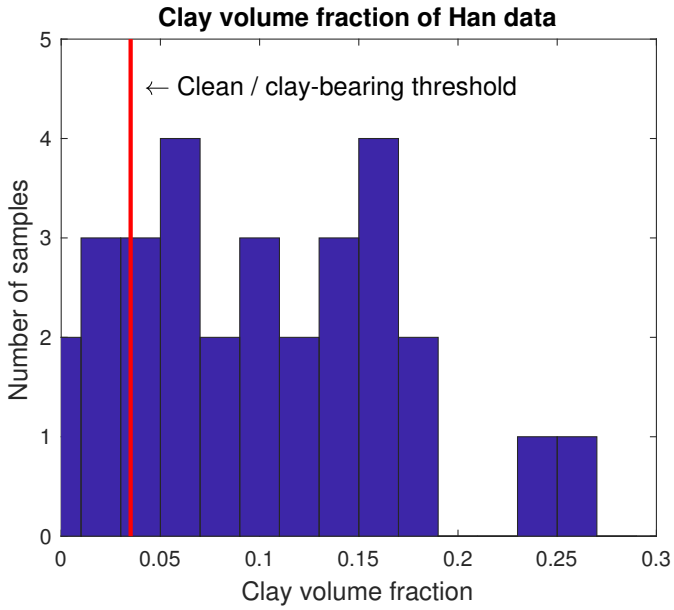

Figure 1: Histogram of the clay content for all samples in the Han data set. The red line at 3.5% clay volume fraction marks the arbitrary cut-off between clean and clay-bearing sandstone samples.

samples have a pure quartz matrix. The clay volume fraction is non-negligible in many samples, as is shown in Figure 1. By modelling the properties of clay-bearing rocks with the assumption of pure quartz matrix, we can test the impact of clay content on the model's parametrisation. All electrical and elastic parameters used in modelling are shown in Table 2.

To investigate the effects of clay on the electrical-elastic model, we partitioned the Han data into clean and clay-bearing data by arbitrarily choosing a threshold of 3.5% clay volume fraction, as shown in Figure 1. This is of interest as the electrical properties of a rock are affected by the presence of clay through the double layer effect (Waxman & Smits, 1968), which the proposed electrical-elastic model does not account for. In addition to this, the elastic moduli of a sandstone can also be significantly affected by only a small amount of clay (Han et al., 1986).

We refer to the model's parameter α as the equivalent pore aspect ratio (EPAR) when applied to real data, following Fournier et al. (2011, 2014, 2018) and Cilli & Chapman (2020). We differentiate between "EPAR" in applied inclusion modelling and "inclusion aspect ratio" in theoretical inclusion modelling because real pores are not ideal spheroids, while the theoretical model's inclusions are.

Table 1: Additional physical properties also modelled by DEM through mathematical equivalency, adapted from Choy (2016).

Problem	Potential, V	$-\nabla V$	Observable	Flux density
Electrostatics	Electric potential	Electric field	Permittivity	Electric displacement
Magnetostatics	Magnetic potential	Magnetic field	Permeability	Magnetic induction
Heat conduction	Temperature	Temperature gradient	Heat conductivity	Heat flux
Diffusion	Density	Density gradient	Diffusion constant	Particle current density

Table 2: Physical parameters used in electrical-elastic modelling.

Constituent	K (GPa)	μ (GPa)	σ $(1/(\Omega\text{m}))$	Moduli source	Conductivity source
Quartz	36.6	45.5	10^{-5}	Mavko et al. (2009)	Han et al. (2011a)
Brine	2.29	0	$1/0.213$	Han et al. (2011a)	Han et al. (2011a)

Table 3: EPAR inversion results for the Han data set and its clean and clay-bearing subsets.

Data set	# Samples	α_{K_0}	α_{μ_0}	*s.d.* (α_{K_0})	*s.d.* (α_{μ_0})	α_K^*	α_μ^*	α_K^*/α_μ^*
All samples	30	17.0	13.0	3.65	1.26	16.4	12.8	1.28
Clean (clay $< 3.5\%$)	6	16.6	12.3	0.78	0.73	16.6	12.3	1.35
Clay-bearing (clay $> 3.5\%$)	24	17.1	13.1	4.07	1.32	16.3	12.9	1.26

To test the electrical-elastic model's performance on the Han data, we first invert equations 18, 19, 22, and 23 for the EPAR associated with each core sample, using the parameters in Table 2 and the measured elastic and electrical data. Rather than solving for a single α which satisfies both bulk and shear modulus measurements in some way, we solve for both the "bulk modulus EPAR", α_K, and "shear modulus EPAR", α_μ, for each sample, by minimising the Root Mean Squared Error (RMSE). Fournier et al. (2011, 2014, 2018) propose α_K and α_μ are the EPARs which minimise the misfit between the modelled and measured bulk modulus and shear modulus data respectively.

In an ideal composite material with a dilute dispersion of spheroidal inclusions, α_K and α_μ of the medium are expected to be equal (Eshelby, 1957). In reality, deviations from the ideal spheroid, or "pore asperities", cause α_K and α_μ to be generally unequal, as observed by Fournier et al. (2011, 2014, 2018) and Cilli & Chapman (2020).

We display the inverted EPARs, α_K and α_μ, for each sample, with their means, α_{K_0} and α_{μ_0}, and 95% confidence intervals in Figures 2 and 3. We also show inversion statistics in Table 3, including the number of samples in each data subset and the standard deviation of the inverted α_K and α_μ for each data subset. Interestingly, we allow the inversion algorithm to search over the full model space $\alpha \in (0, \infty)$ and find it consistently favours modelling with prolate spheroidal pores, where $\alpha > 1$.

To calculate the optimal model parameters, α_K^* and α_μ^*, we used the average solutions, α_{K_0} and α_{μ_0}, as starting points in non-linear global optimisations which minimised the bulk or shear modulus misfit for all samples. These optimal EPARs are also shown in Table 3. There is a 1.8% difference in α_K^* and a 4.7% difference in α_μ^* between clean and clay-bearing model parametrisations. Thus, we conclude α_K^* and α_μ^* are weakly influenced by clay volume fraction in this data set. The ratio of α_K^* and α_μ^* in this electrical-elastic DEM modelling exercise is also shown in Table 3, and interestingly is not unity, which is an observation previously made only in purely elastic modelling settings.

We forward modelled resistivity-bulk modulus and resistivity-shear modulus trends using α_K^* and α_μ^* respectively, as shown in Figure 4. The propagated 95% confidence intervals from the sample-by-sample EPAR inversions of Figures 2 and 3 are also shown. The joint electrical-elastic Hashin-Shtrikman bounds (Carcione et al., 2007) are displayed, with the proposed electrical-elastic modelling method obeying these bounds in all examples. Being asymptotically correct, the electrical-elastic DEM model converges to the water moduli at 100% porosity and the resistivity of water, and converges to the matrix moduli at zero porosity and

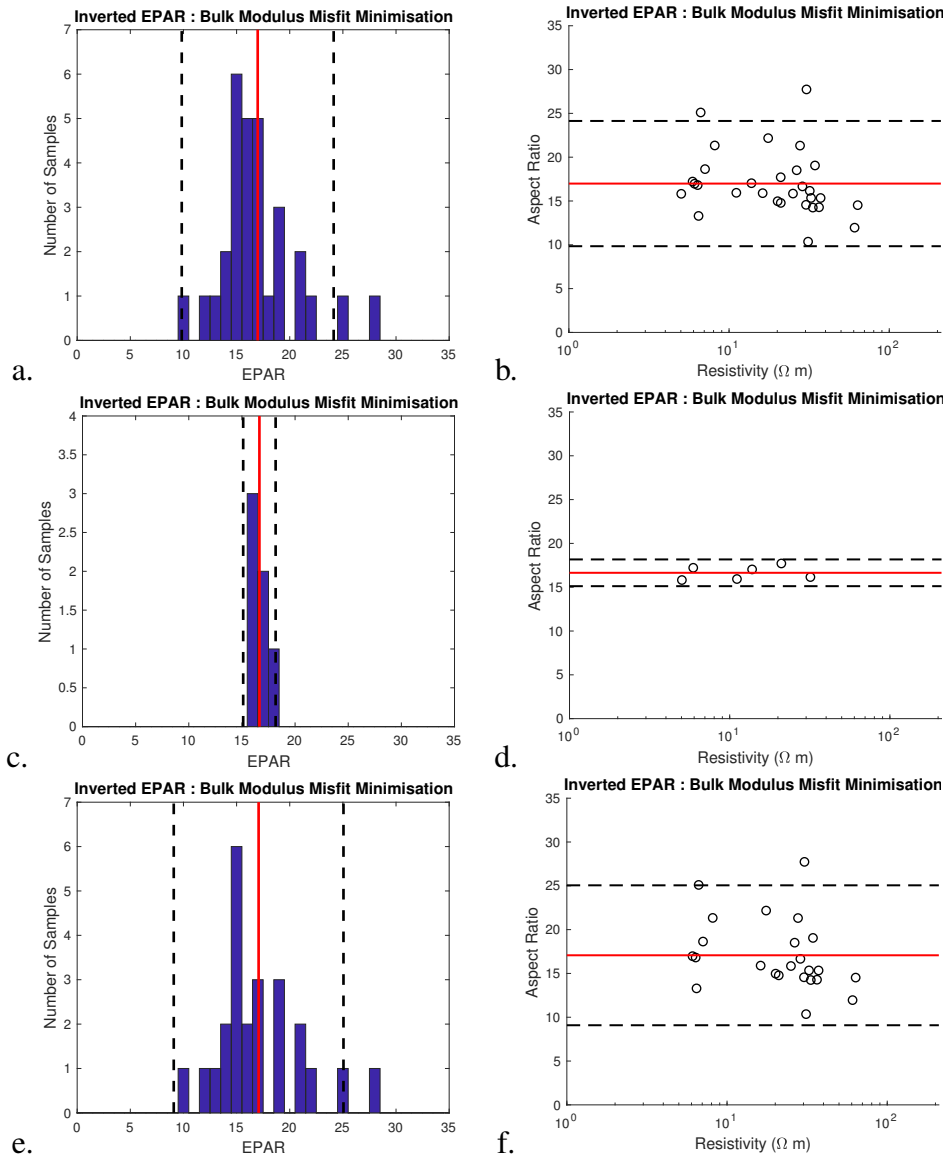

Figure 2: Inverted α_K for each core sample by minimising misfit between measured and modelled bulk modulus. Subfigures a and b show all data; c and d show clean data; and e and f show clay-bearing data. Subfigures a, c, and e show histograms of inversion results, while subfigures b, d, and f show the inverted results against measured sample resistivity. The mean EPAR for each data set is shown (red line), as well as the solution's 95% confidence intervals (dashed black).

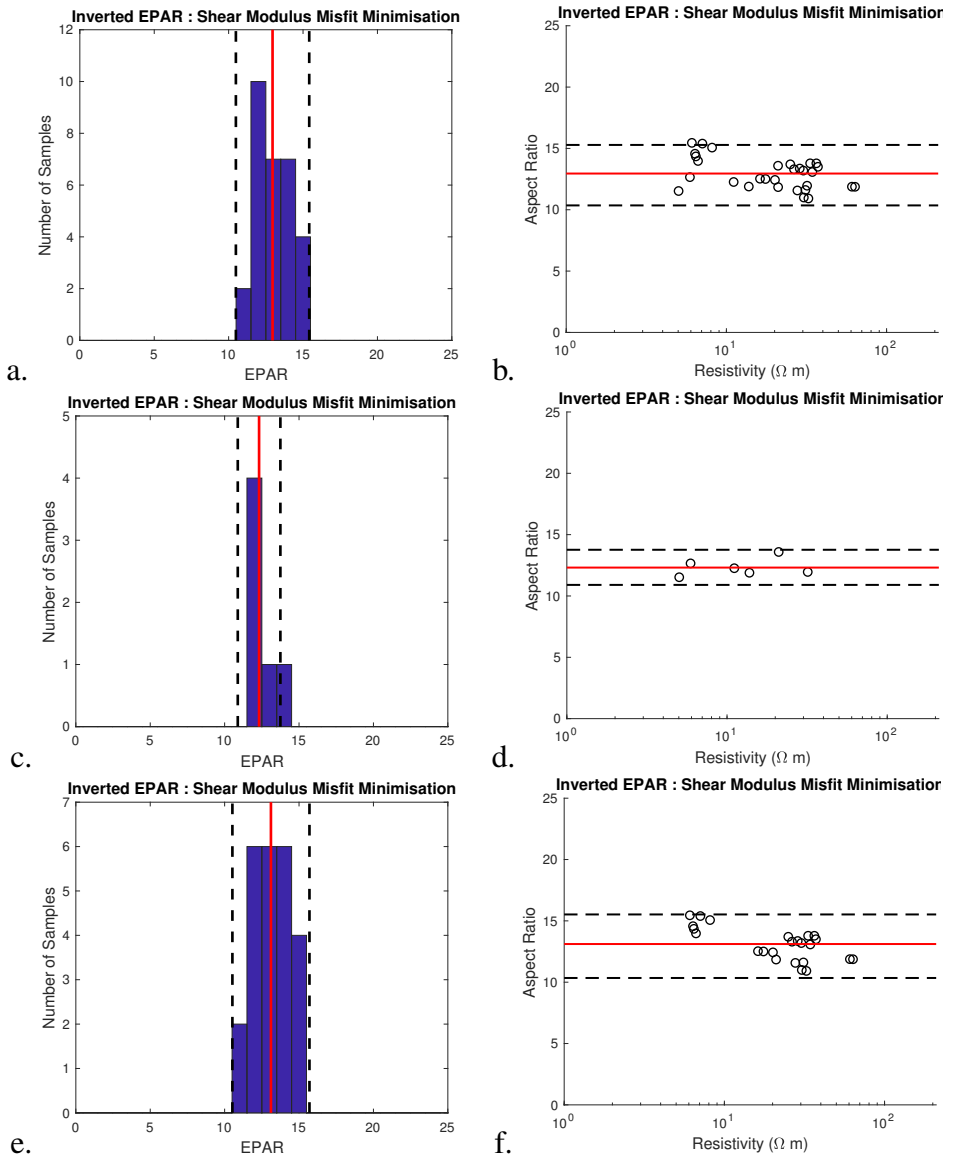

Figure 3: Inverted α_μ for each core sample by minimising misfit between measured and modelled bulk modulus. Subfigures a and b show all data; c and d show clean data; and e and f show clay-bearing data. Subfigures a, c, and e show histograms of inversion results, while Subfigures b, d, and f show the inverted results against measured sample resistivity. The mean EPAR for each data set is shown (red line), as well as the solution's 95% confidence intervals (dashed black).

the resistivity of matrix material. We note the matrix resistivity is not shown on Figure 4 and so the low-porosity, asymptotic modulus values (red diamonds) do not coincide with the forward modelled trend line in the figure.

3.2 V_p/V_s Modelling

The ratio of a rock's P- and S-wave velocities is of importance in reservoir characterisation as different fluids can have similar shear wave velocities but vastly different compressional velocities. The V_p/V_s ratio of any given rock is also highly sensitive to the rock's porosity due to the often large differences between pore fluid and mineral velocities. Using the electrical-elastic model presented above, we now predict a rock's V_p/V_s ratio using only electrical measurements, an empirical velocity-density relation, and the model's known parameters, assumed *a priori* to be pre-calibrated.

We consider modelling a V_p/V_s ratio trend through the entire Han data set. The first step is modelling elastic moduli trends (Figures 4a,b) using parameters $\alpha_K^* = 16.4$ and $\alpha_\mu^* = 12.8$ (Table 3). V_p and V_s can then be calculated using the linear elasticity equations and the empirical Gardner (Gardner et al., 1974) relation for sandstones:

$$\rho = 0.31 V_p^{0.25} \,. \tag{24}$$

We use an empirical density-velocity relation here to demonstrate how a V_p/V_s ratio trend can be estimated solely using electrical measurements. However, the use of reliable density measurements, if possible, should lead to more accurate V_p/V_s predictions.

Figure 5 shows a crossplot of the measured V_p and V_s data, as well as the V_p and V_s trends forward modelled from formation factors spanning some subset of the interval $FF \in]2, 1000[$. Residuals in V_p and V_s have standard deviations of 186 m/s and 151 m/s respectively. The standard deviation of the residuals in V_p/V_s ratio is 0.060. The empirical model for clay-bearing sandstones of Han et al. (1986) is shown for comparison. The empirical trend provides a better fit to the data at lower velocities, however it is calibrated on many samples, with shear velocities ranging from less than 1500 m/s to over 3500 m/s. Because of this severe difference in model calibration, we cannot conclude the empirical trend of Han et al. (1986) is actually a better model than the proposed electrical-elastic model.

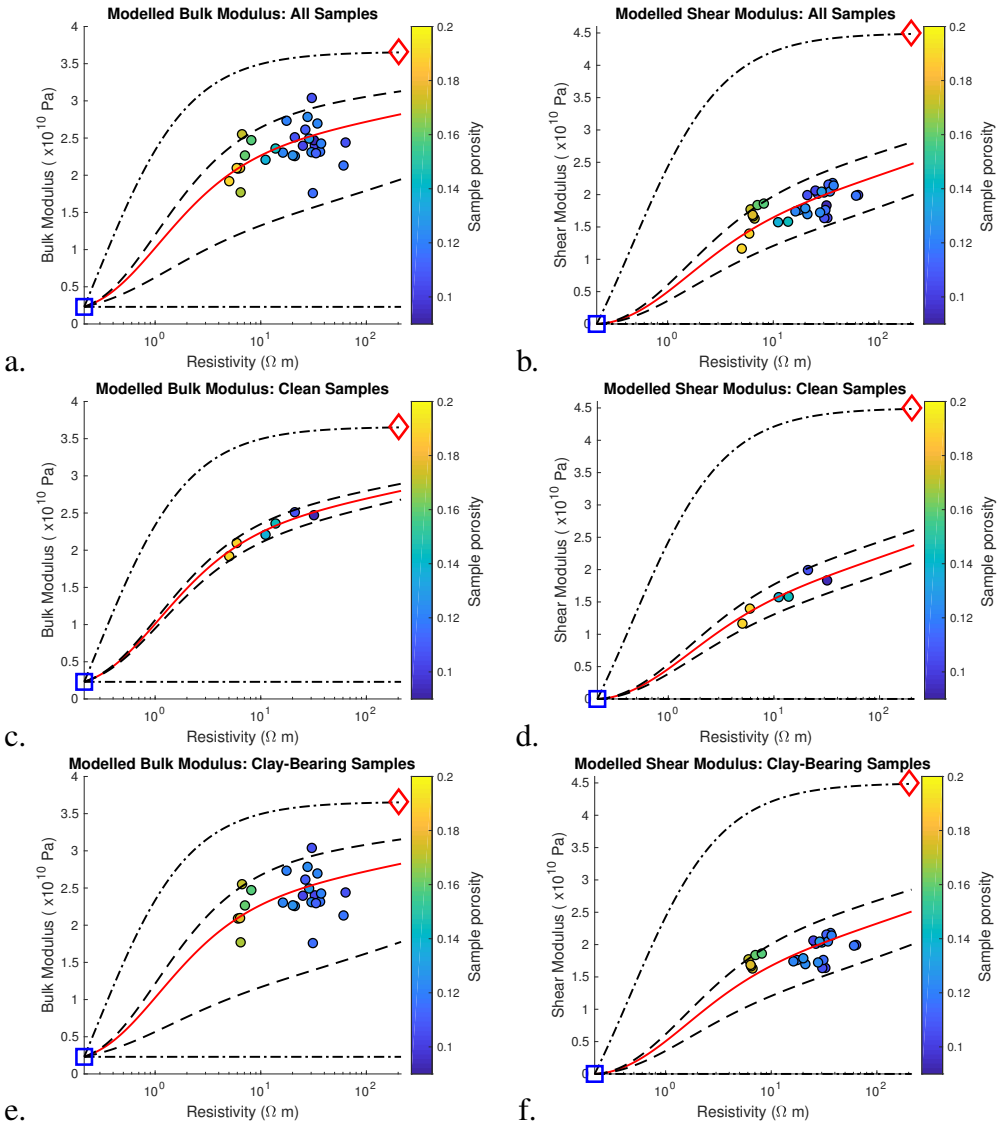

Figure 4: The electrical-elastic measurements (circles) of the Han data set and its clean and clay-bearing sample subsets are modelled by the proposed joint electrical-elastic DEM expressions (red trends) using optimal aspect ratios shown in Table 3. Bulk modulus (left column) and shear modulus (right column) are modelled using parameters α_K^* and α_μ^* respectively. The 95% confidence intervals on initial EPAR estimates, shown in Figures 2 and 3, are forward modelled (dashed curves). The electrical-elastic upper and lower Hashin-Shtrikman bounds are displayed (dot-dashed curves). The electrical-elastic model converges exactly to the properties of water (blue square) at 100% porosity and $\sigma^* = \sigma_2$. It also converges to the properties of matrix material when $\sigma^* = \sigma_1$ and porosity is zero (asymptotic modulus value shown by red diamond). Measured sample porosity (marker colour) is also shown for context. 18

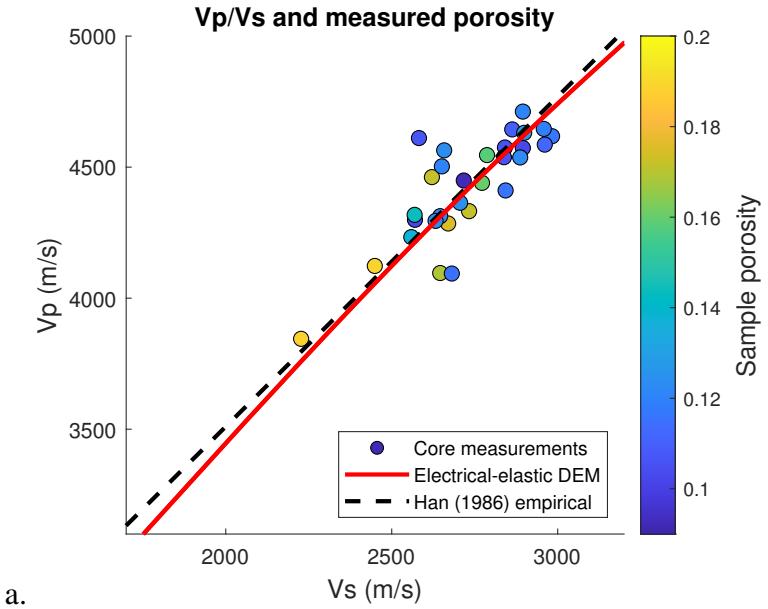

a.

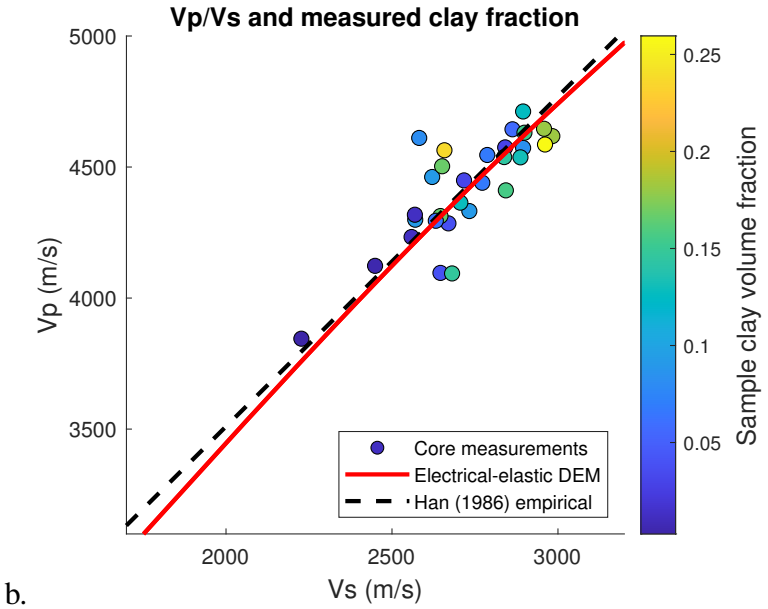

b.

Figure 5: The measured velocities of the Han data set (circles), filled with each sample's a) measured porosity, and b) measured clay volume fraction. The solid red curve shows the V_p/V_s trend predicted by the electrical-elastic DEM model using only resistivity measurements, the empirical Gardner equation, and a prior model calibration. The dashed black line shows the empirical trend of Han et al. (1986) for mixed clay sandstones.

4 Discussion

The advantage of cross-property DEM modelling is its ability to characterise a rock's physical properties with fewer measurements. For example, in the case that sonic and porosity well logs are unavailable, it may be possible to estimate V_p/V_s ratios at depth using resistivity well logs only, as was demonstrated with laboratory data in Figure 5. By requiring fewer types of measurements to characterise the physical properties of a rock, we may be able to save on data acquisition time and costs. On top of this, we may also be able to infer new information from legacy data sets. For example, we may be able to estimate the elastic properties of core samples which only had electrical resistivity measurements made upon them at the time of experimentation.

An outstanding problem in applied inclusion modelling is the disparity between α_K and α_μ in real rocks. This difference may be due to the fact that the DEM equations which model K and μ are coupled differential equations, unlike those which model the other physical properties discussed herein. In light of this, there is scope for future research to test the universality of the aspect ratio parameter across different cross-property models, as opposed to the difference between α_K and α_μ, which is a difference between two parameters applied to the same model. That is, this research leads us to a testable hypothesis: The cross-property DEM parameter, aspect ratio, is universal when linking a given rock's various physical properties.

The proposed electrical-elastic DEM modelling method's preference to approximate pores using prolate spheroids contrasts with typical elastic modelling flows, where pores are often represented by oblate spheroids. Modelling elastic properties with oblate spheroidal inclusions in a DEM framework coincides with the lower Hashin-Shtrikman bound (Norris, 1985), while modelling with prolate spheroids does not. This may suggest that prolate spheroids may only be preferable for electrical-elastic modelling so long as the rock's moduli are sufficiently high.

Figures 2 and 3 show a large scatter in α_K for the clay-bearing data sets. The EPAR parameter in a DEM model is a fitting parameter, absorbing inaccuracies in clay-related parameters, assumptions and the independent variable. The presence of scatter in EPAR when inverted from clay-bearing samples but not clean samples indicates variability in other model parameters or inaccurate assumptions, such as assuming a pure quartz mineralogy or not accounting for the double layer effect.

The scatter in inverted EPARs (Figures 2 and 3) for clay bearing samples is significantly lower in the inversion for α_μ than for α_K. This suggests there is

higher modelling uncertainty due to clay content in estimating the effective bulk modulus than shear modulus. Table 3 shows the standard deviation in inverted α_{μ_0} for clean samples and the full data set are very similar. It therefore seems the uncertainty in modelled shear modulus is weakly sensitive to clay content in the Han data.

The presented model accounts for an isotropic stiffness and conductivity, where the electrical and elastic properties are fully described by scalar moduli, rather than electrical resistivity and stiffness tensors. Extending this model to the anisotropic case may be useful, as Singh et al. (2020) showed using digital rocks that elastic anisotropy leads to a different EPAR depending on the direction of sonic measurement. This anisotropic extension of the model could be of interest as North & Best (2014) showed that even visually isotropic sandstones can have up to 25% anisotropy due to syn-depositional and post-depositional compaction processes.

We have presented an electrical-elastic DEM model which is tested by predicting a rock's elastic properties from electrical measurements. However, we do not predict electrical properties from elastic measurements. This is because the model comprises of coupled differential equations which are solved numerically; one equation relates bulk modulus, while the other relates shear modulus, to electrical measurements. Inverting these coupled differential equations to solve for electrical conductivity from both measured bulk and shear moduli is significantly more difficult, if at all possible, and not considered here.

Due to this dubious calculability of any physical properties from measured elastic moduli, we are speculatively presenting here 25 mappings between physical properties: that is, from 5 physical properties (electrical resistivity and those in Table 1) to the remaining five properties, which includes elastic moduli. If the mapping from elastic moduli to other properties were also calculable, this number would increase to 30 distinct mappings. The potential application of many of these mappings will not necessarily be in rock physics, where we are predominantly concerned with a rock's elastic and electrical properties. Rather, we expect the application of some of these models to be in other fields where inclusion modelling is used for composite materials, for example in the engineering or materials sciences.

5 Conclusion

We argue that reformulating a pre-existing electrical effective medium model allows us to derive new electrical-elastic DEM expressions which effectively model

public domain, clay-bearing sandstone measurements. Many electrical-elastic modelling workflows require an estimation of porosity as an intermediate step, however the proposed cross-property DEM expressions require no porosity information for evaluation. Being a DEM model, these proposed expressions are correct in the high and low porosity limit, unlike many empirical electrical-elastic models. Modelling V_p/V_s from resistivity measurements has been challenging to date due to the difficulty of shear modulus modelling from electrical measurements, however the proposed electrical-elastic DEM modelling method models both V_p and V_s data for laboratory measurements, showing potential for improved V_p/V_s modelling from resistivity data. Although a rock's elastic moduli and resistivity are known to be significantly affected by clay content, it seems the multiphysics DEM model's single parameter is only weakly affected by clay volume fraction in the measured laboratory data, showing promise for robust cross-property modelling in lithologies with unknown or variable clay content. Given the mathematical equivalence of inclusion modelling when estimating a medium's elastic moduli, electrical conductivity, electrical permittivity, thermal conductivity, magnetic permeability, and diffusion constant, we see potential for the proposed concept of cross-property DEM to be more broadly applied in the cross-property modelling of composite materials.

Acknowledgments

The authors would like to thank Petrobras and Shell for their sponsorship of the International Center for Carbonate Reservoirs (ICCR), and for permission to publish this work from the VSP project. We thank Andrew Curtis, Ian Main, Rachel Wood, Anton Ziolkowski, and Giorgos Papageorgiou at the University of Edinburgh, Tongcheng Han at the China University of Petroleum, Qingdao, Angus Best at the UK National Oceanograpy Center, Southampton, and Tony Watts at the University of Oxford for their support in this work. The data on which this paper is based can be obtained in Han et al. (2011b).

A Cross-Property DEM Modelling for Thermal Conductivity

The mathematical equivalence of a composite's estimated effective electrical conductivity and thermal conductivity in the case of inclusion modelling (Berryman,

1995; Choy, 2016) allows us to write the DEM expression of a two-phase composite's effective thermal conductivity κ^* using the form of equation 13 as:

$$\frac{d\kappa^*}{d\phi} = 3\kappa^* \frac{(\kappa_2 - \kappa^*)\,\mathcal{T}^{(*2)}}{(1-\phi)}\,. \tag{25}$$

where κ_2 is inclusion thermal conductivity, and $\mathcal{T}^{(*2)}$ is defined analogously to $R^{(*2)}$ as:

$$\mathcal{T}^{(*2)} = \frac{1}{9}\left[\frac{4}{\kappa^* + \kappa_2 + L\,(\kappa^* - \kappa_2)} + \frac{1}{\kappa^* - L\,(\kappa^* - \kappa_2)}\right]. \tag{26}$$

Equation 25 is solved with boundary condition $\kappa^*\,(\phi = 0) = \kappa_1$, where κ_1 is the background thermal conductivity.

Applying the chain rule to equations 9 and 25, the change in the electrical conductivity with respect to thermal conductivity is thus:

$$\frac{d\sigma^*}{d\kappa^*} = \frac{\sigma^*\,(\sigma_2 - \sigma^*)}{\kappa^*\,(\kappa_2 - \kappa^*)} \frac{R^{(*2)}}{\mathcal{T}^{(*2)}}\,; \tag{27}$$

with boundary condition $\sigma^*\,(\kappa^* = \kappa_1) = \sigma_1$. The model for thermal conductivity as a function of electrical conductivity is the reciprocal of equation 27 using the boundary conditions $\kappa^*\,(\sigma^* = \sigma_1) = \kappa_1$.

Similarly, the change in the elastic moduli of a composite material with respect to its thermal conductivity is modelled by the coupled equations:

$$\frac{dK^*}{d\kappa^*} = \frac{1}{3\kappa^*}\left(\frac{K_2 - K^*}{\kappa_2 - \kappa^*}\right)\frac{P^{(*2)}}{\mathcal{T}^{(*2)}}\,; \tag{28}$$

$$\frac{d\mu^*}{d\kappa^*} = \frac{1}{3\kappa^*}\left(\frac{\mu_2 - \mu^*}{\kappa_2 - \kappa^*}\right)\frac{Q^{(*2)}}{\mathcal{T}^{(*2)}}\,. \tag{29}$$

with boundary conditions $K^*\,(\kappa^* = \kappa_1) = K_1$ and $\mu^*\,(\kappa^* = \kappa_1) = \mu_1$.

As in the electrical-elastic case, equations 27 to 29 contain no inclusion volume fraction terms yet are correct in the high and low inclusion volume fraction asymptotes.

References

Alcocer, J. E., García, M. V., Soto, H. S., Baltar, D., Paramo, V. R., Gabrielsen, P. T., & Roth, F., 2013. Reducing uncertainty by integrating 3D CSEM in the Mexican deep-water exploration workflow, *First Break*, **31**(4), 75–79.

Archie, G. E., 1942. The electrical resistivity log as an aid in determining some reservoir characteristics, *Transactions of the AIME*, **146**(1), 54–62.

Berryman, J. G., 1980. Long-wavelength propagation in composite elastic media II. Ellipsoidal inclusions, *The Journal of the Acoustical Society of America*, **68**(6), 1820–1831.

Berryman, J. G., 1992. Single-scattering approximations for coefficients in Biot's equations of poroelasticity, *The Journal of the Acoustical Society of America*, **91**(2), 551–571.

Berryman, J. G., 1995. Mixture theories for rock properties, *Rock physics and phase relations: A handbook of physical constants*, **3**, 205–228.

Bruggeman, V. D., 1935. Berechnung verschiedener physikalischer konstanten von heterogenen substanzen. i. dielektrizitätskonstanten und leitfähigkeiten der mischkörper aus isotropen substanzen, *Annalen der Physik*, **416**(7), 636–664.

Carcione, J. M., Ursin, B., & Nordskag, J. I., 2007. Cross-property relations between electrical conductivity and the seismic velocity of rocks, *Geophysics*, **72**(5), E193–E204.

Chapman, M., Zatsepin, S. V., & Crampin, S., 2002. Derivation of a microstructural poroelastic model, *Geophysical Journal International*, **151**(2), 427–451.

Chen, J. & Dickens, T. A., 2009. Effects of uncertainty in rock-physics models on reservoir parameter estimation using seismic amplitude variation with angle and controlled-source electromagnetics data, *Geophysical Prospecting*, **57**(1), 61–74.

Choy, T., 2016. *Effective Medium Theory: Principles and Applications*, International Series of Monographs on Physics, Oxford University Press.

Cilli, P. & Chapman, M., 2020. The power-law relation between inclusion aspect ratio and porosity: Implications for electrical and elastic modeling, *Journal of Geophysical Research: Solid Earth*, **125**(5), 1–25.

Dvorkin, J. & Nur, A., 1993. Dynamic poroelasticity: A unified model with the squirt and the Biot mechanisms, *Geophysics*, **58**(4), 524–533.

Engelmark, F., 2010. Velocity to resistivity transform via porosity, in *SEG Technical Program Expanded Abstracts 2010*, pp. 2501–2505, Society of Exploration Geophysicists.

Eshelby, J. D., 1957. The determination of the elastic field of an ellipsoidal inclusion, and related problems, *Proceedings of the Royal Society of London A*, **241**(1226), 376–396.

Fournier, F., Léonide, P., Biscarrat, K., Gallois, A., Borgomano, J., & Foubert, A., 2011. Elastic properties of microporous cemented grainstones, *Geophysics*, **76**(6), E211–E226.

Fournier, F., Léonide, P., Kleipool, L., Toullec, R., Reijmer, J. J., Borgomano, J., Klootwijk, T., & Van Der Molen, J., 2014. Pore space evolution and elastic properties of platform carbonates (Urgonian limestone, Barremian–Aptian, SE France), *Sedimentary Geology*, **308**, 1–17.

Fournier, F., Pellerin, M., Villeneuve, Q., Teillet, T., Hong, F., Poli, E., Borgomano, J., Léonide, P., & Hairabian, A., 2018. The equivalent pore aspect ratio as a tool for pore type prediction in carbonate reservoirs, *AAPG Bulletin*, **102**(7), 1343–1377.

Frank, V., 1963. On the penetration of a static homogeneous field in an anisotropic medium into an ellipsoidal inclusion consisting of another anisotropic medium, in *Electromagnetic theory and antennas*, pp. 615–623, ed. Jordan, E. C., The Macmillan Co., New York.

Gardner, G. H. F., Gardner, L. W., & Gregory, A. R., 1974. Formation velocity and density: The diagnostic basics for stratigraphic traps, *Geophysics*, **39**(6), 770–780.

Glover, P. W., 2016. Archie's law - a reappraisal, *Solid Earth*, **7**(4), 1157–1169.

Hamada, G., 2004. Reservoir fluids identification using vp/vs ratio?, *Oil & Gas Science and Technology*, **59**(6), 649–654.

Han, D.-h., Nur, A., & Morgan, D., 1986. Effects of porosity and clay content on wave velocities in sandstones, *Geophysics*, **51**(11), 2093–2107.

Han, T., Best, A. I., MacGregor, L. M., Sothcott, J., & Minshull, T. A., 2011a. Joint elastic-electrical effective medium models of reservoir sandstones, *Geophysical Prospecting*, **59**(4), 777–786.

Han, T., Best, A. I., Sothcott, J., & MacGregor, L. M., 2011b. Joint elastic-electrical properties of reservoir sandstones and their relationships with petrophysical parameters, *Geophysical Prospecting*, **59**(3), 518–535.

Han, T., Clennell, M. B., Cheng, A. C. H., & Pervukhina, M., 2016. Are self-consistent models capable of jointly modeling elastic velocity and electrical conductivity of reservoir sandstones?, *Geophysics*, **81**(4), D377–D382.

Hussien, M. N. & Karray, M., 2015. Shear wave velocity as a geotechnical parameter: an overview, *Canadian Geotechnical Journal*, **53**(2), 252–272.

Jensen, E. H., Gelius, L.-J., Johansen, T. A., & Wang, Z., 2013. Consistent joint elastic-electrical differential effective-medium modelling of compacting reservoir sandstones, *Geophysical Prospecting*, **61**(4), 788–802.

Jones, A. G., Fishwick, S., Evans, R. L., Muller, M. R., & Fullea, J., 2013. Velocity-conductivity relations for cratonic lithosphere and their application: Example of southern africa, *Geochemistry, Geophysics, Geosystems*, **14**(4), 806–827.

Kennett, B., Widiyantoro, S., & Van Der Hilst, R., 1998. Joint seismic tomography for bulk sound and shear wave speed in the earth's mantle, *Journal of Geophysical Research: Solid Earth*, **103**(B6), 12469–12493.

Kwon, M. J. & Snieder, R., 2011. Uncertainty analysis for the integration of seismic and controlled source electro-magnetic data, *Geophysical Prospecting*, **59**(4), 609–626.

Mavko, G. & Jizba, D., 1991. Estimating grain-scale fluid effects on velocity dispersion in rocks, *Geophysics*, **56**(12), 1940–1949.

Mavko, G., Mukerji, T., & Dvorkin, J., 2009. *The rock physics handbook: Tools for seismic analysis of porous media*, Cambridge University Press.

Maxwell Garnett, J. C., 1904. Colours in metal glasses and in metallic films, in *Proceedings of the Royal Society of London*, vol. 73, pp. 443–445, Royal Society of London.

Mendelson, K. S. & Cohen, M. H., 1982. The effect of grain anisotropy on the electrical properties of sedimentary rocks, *Geophysics*, **47**(2), 257–263.

Norris, A. N., 1985. A differential scheme for the effective moduli of composites, *Mechanics of Materials*, **4**(1), 1–16.

North, L. J. & Best, A. I., 2014. Anomalous electrical resistivity anisotropy in clean reservoir sandstones, *Geophysical Prospecting*, **62**(6), 1315–1326.

Osborn, J. A., 1945. Demagnetizing factors of the general ellipsoid, *Physical Review*, **76**(11-12), 351–357.

Polder, D. & Van Santeen, J., 1946. The effective permeability of mixtures of solids, *Physica*, **12**(5), 257–271.

Salem, H. S. & Chilingarian, G. V., 1999. The cementation factor of Archie's equation for shaly sandstone reservoirs, *Journal of Petroleum Science and Engineering*, **23**(2), 83–93.

Sen, P. N., Scala, C., & Cohen, M. H., 1981. A self-similar model for sedimentary rocks with application to the dielectric constant of fused glass beads, *Geophysics*, **46**(5), 781–795.

Singh, J., Cilli, P., Hosa, A., & Main, I., 2020. Digital rock physics in four dimensions: simulating cementation and its effect on seismic velocity, *Geophysical Journal International*, **222**(3), 1606–1619.

Wang, Z. & Gelius, L.-J., 2010. Electric and elastic properties of rock samples: A unified measurement approach, *Petroleum Geoscience*, **16**(2), 171–183.

Waxman, M. H. & Smits, L. J. M., 1968. Electrical conductivities in oil-bearing shaly sands, *Society of Petroleum Engineers Journal*, **8**(02), 107–122.

Werthmüller, D., Ziolkowski, A., & Wright, D., 2013. Background resistivity model from seismic velocities, *Geophysics*, **78**(4), E213–E223.

Yasir, S., Abbas, H., & Jani, J., 2018. Estimation of soil young modulus based on the electrical resistivity imaging (eri) by using regression equation, in *AIP Conference Proceedings*, vol. 2020, p. 020071, AIP Publishing LLC.